Pro gradu -thesis

Characterization of dry-film photolithography for the study of *B. burgdorferi* motility

Arttur Pudas

University of Jyväskylä

The Department of Biological and

Environmental Science

1.10.2017

Preface

The laboratory experiments of this thesis were carried out in Leona Gilbert's research team at the University of Jyväskylä in Department of Biological and Environmental Science and Nanoscience center. I would like to thank Dr. Nitipon Puttaraksa and Dr. Leona Gilbert for their advice and support as the supervisors. In addition I would like to thank Laura Pitkänen, Kimmo Kinnunen, Hannu Salo, and Tarmo Suppula for their assistance as laboratory technicians and engineers. I would also like to thank everyone in the research group, but especially Kati Karvonen, Renée Hoban, and Martin Chillman for guiding me with certain laboratory protocols and providing guidance.

Jyväskylän yliopisto **Pro gradu –tutkielman tiivistelmä**
Matemaattis-luonnontieteellinen tiedekunta

Tekijä: **Arttur Pudas**
Tutkielman nimi: Kuivafilmilitografian karakterisointi *Borrelia burgdorferi:n liikkuvuuden tutkimiselle*
English title: Characterization of dry-film photolithography for the study of *Borrelia burgdorferi* motility
Päivämäärä: 30.7.2017 **Sivumäärä:** 31

Laitos: Bio- ja ympäristötieteiden laitos
Oppiaine: Solubiologia
Tutkielman ohjaaja(t): Leona Gilbert ja Nitipon Puttaraksa

Borrelia burgdorferi on puutiaisten kantama spirokeettabakteeri, joka voi tarttua useisiin eläinlajeihin. Ihmisillä *B. burgdorferi* aiheuttaa borrelioosia. Tauti on laajalle levinnyt monissa pohjois- ja länsimaissa ja leviää entisestään ilmastonmuutoksen laajentaessa punkkien elinaluetta. Monet tekijät vaikeuttavat borrelioosin hoitoa. *B. burgdorferin* kyky välttää ihmisen luontaista immuunijärjestelmää ovat tässä suhteessa merkittävä. Bakteerien liikkuvuus on olennainen tämän kyvyn kannalta, mutta sen tarkka rooli bakteerien kyvyssä liikkua verisuonistossa on osittain tuntematon.

Mikrofluidistiikka hyödyntää tiettyjä nesteiden dynamiikkaa ohjaavia voimia, jotka aiheuttavat nesteitä ja niiden kantamia partikkeleita käyttäytymään eri tavoin mikroskooppisessa ympäristössä makroskooppisiin ympäristöihin verrattuna. Valmistustekniikoiden edistyminen on mahdollistanut mikrofluidiikan etujen hyväksikäytön lisääntymisen ja edesauttanut sen kasvua voimakkaana biologisten tieteiden välineenä. Kuivakalvo-litografia tarjoaa helppokäyttöisen ja edullisen vaihtoehdon perinteisille mikrofluidisille valmistusmenetelmille, jotka edellyttävät puhdastiloja. Mikrofluidisten sirujen valmistukseen voidaan käyttää polydimetyylisiloksaani-polymeeria (PDMS), joka on joustava, bioyhteensopiva ja yksinkertaistaa valmistusprosessia. Mikrofluidistiikka soveltuu erinomaisesti verisuonien, imusuonijärjestelmän ja muiden *in vivo* -järjestelmien, simulointiin.

Tämän tutkimuksen tarkoituksena oli optimoida kuivakalvolitografiamenetelmä biologisissa kokeissa käytettäväksi ja suorittaa mikrofluidinen virtauskoe käyttäen eläviä *B. burgdorferi* soluja. Mikrofluidinen valmistusmenetelmä perustui mustesuihkutulostuksella tehtyihin peittomaskeihin. Kuparilevyt, joissa oli DuPont Riston 200 -sarjan negatiivinen fotoresistipäällystys, liitettiin maskeihin ja altistettiin UV:lle läheisyyslitografialla. Lopulliset mikofluidiset sirut valmistettiin PDMS:stä ja liitettiin lasipinnalle aktivoimalla sekä lasi että PDMS-pinnat plasmalla. Valmistusmenetelmä karakterisoitiin pyyhkäisyelektroni- ja stereomikroskopialla. Vihreää fluoresoivaa proteiinia tuottava *B. burgdorferi* GCB726 kanta syötettiin mikrokanavaan eri virtausnopeuksilla, jotka olivat korkeintaan 0,1 ml/min. Bakteerien liikkuvuus videoitiin fluoresenssimikroskopialla.

Kuivakalvolitografian avulla mikrokanavat voitiin valmistaa luotettavasti 75 µm läpimittaan asti alle 5 tunnin kuluessa peittomaskin valmistuksesta. Vaikka kanavissa havaittiin pieniä vikoja, niiden vaikutus laminaariseen virtaukseen oli vähäpätöinen. Kuvataajuuden rajoitteiden vuoksi *B. burgdorferi* videokuva-aineistosta käytettiin vain 0,0073 cm/s:n virtausnopeudella tallennettuja videoita. *B. burgdorferin* liikkuvuus ilmeni kolmella tavalla: "Tanssimisessa", voltteina ja vuorovaikutuksena kanavan seinämän kanssa.

Suurin osa mikrofluidisten sirujen valmistusprosesseissa havaituista vioista johtui läheisyyslitografiamenetelmän ja mustesuihkutulostimen rajoista. Tuloksia voitaisiin parantaa litografiaa optimoimalla ja parempi laatuisella maskitulostimella. Mikrosiruvalmistusprosessi oli tyydyttävä *B. burgdorferin* virtauksessa käyttäytymisen tarkkailemiseksi. *B. burgdorferin* liikkuvuus vaikutti aktiivisesti bakteerisolujen orientaatioon laminaarisessa virtauksessa, mikä johti hypoteesiin, että tämä liikkuvuus voisi antaa soluille mahdollisuuden uida verisuonijärjestelmässä. Lisätutkimuksia tarvitaan varmistamaan, onko tämä kardiovaskulaarinen liikkuvuus kehittynyt nimenomaan ratkaisevaksi ektravasaatiossa vai pelkkä välituote solujen kyvystä liikkua pehmytkudoksissa. Nämä tulokset osoittavat kuitenkin, että *B. burgdorferin* liikkuvuus saattaa auttaa bakteeria löytämään verisuonten seinä ekstravasaation aikana.

University of Jyväskylä
Faculty of Mathematics and Science

Abstract of Master´s Thesis

Author: **Arttur Pudas**
Title of thesis: Characterization of dry-film photolithography for the study of *Borrelia burgdorferi* motility
Finnish title: Kuivafilmilitografian karakterisointi *Borrelia burgdorferi:n liikkuvuuden tutkimiselle*
Date: 30.7.2017 **Pages:** 31

Department: Department of Biological and Environmental Science
Chair: Cell Biology
Supervisor(s): Leona Gilbert and Nitipon Puttaraksa

Borrelia burgdorferi is a species of sphirochete bacteria infecting multiple different species of animals via a tick vector. In humans *B. burgdorferi* causes lyme disease. In many northern and western countries the disease has advanced to an endemic state, and is spreading further due to climate change affecting the spread of its carrier vector. Many factors contribute to the difficulty controlling *B. burgdorferi* infections and Lyme disease. One of the main factors are the methods through which the bacteria are able to evade the immune system. The bacterial mobility of *B. burgdorferi* is a large contributing factor to this ability, but the extent to which this mobility is crucial in the extravasation step in its pathogenic life cycle remains partially unknown.

Microfluidics takes advantage of the different scale dependencies of certain forces governing fluid dynamics that causes the fluids and particles within to behave differently in a microscale environment compared to the traditional macroscale. Advances in fabrication techniques have made utilizing the advantages of microfluidic techniques more widespread and enabled it to potentially grow into a powerful tool for biological sciences. Dry-film photolithography offers ease of use and a cheap alternative to traditional microfluidic fabrication methods which require access to clean room facilities. These microfluidic chips can be made with flexible polydimethylsiloxane (PDMS) polymer, which is biocompatible, and makes the fabrication process relatively simple. Microfluidics is ideally suited for simulating cardiovascular environments, and other *in vivo* systems, such as the lymphatic system.

The aim of this study was to characterize and optimize a dry-film photolithography method for use in biological experiments, and to carry out a flow experiment using living *B. burgdorferi* cells. The microfluidic fabrication technique relied on masks made with inkjet printing. Pre laminated copper plates with DuPont Riston 200 series negative photoresist were then coupled with the masks and exposed under UV with a proximity lithography method. The final chips were manufactured in PDMS, and coupled with a glass substrate by activating both the glass and PDMS surfaces with air plasma. The fabrication method was characterized with scanning electron microscopy and stereo microscopy. A green fluorescent protein expressig strain of *B. burgdorferi* GCB726 flown in a microchannel at flow rates of up to 0.1 ml/min. Video footage of these experiments were captured with fluorescent microscopy technique.

With the dry-film photolithography technique microchannel structures could be reliably fabricated down to 75 µm resolution in less than 5 h from the mask fabrication to the final product. Though small defects were observed in the channel their effect on the laminar flow was negligible. Due to framerate constreaints only footage of *B. burgdorferi* in 0.0073 cm/s flow speed used. *B. burgdorferi* mobility in flow was observed in three distinct patterns: ‘Dancing’, flipping, and interacting with the channel wall.

Most of the defects observed in the microfluidic chip fabrication processes were due to intrinsic to our proximity photolithography set-up and limits of the ink-jet printer. However, the results could be improved by further optimizing the photolithography set-up and with higher quality mask printing. The microchip fabrication process was satisfactory for the fast and cheap production of microfluidic experiment set-ups to observe *B. burgdorferi* in flow. The mobility of *B. burgdorferi* actively changed the orientation of the bacterial cells in laminar flow, which lead to the hypothesis that their mobility could confer the cells an ability to swim in the cardiovascular system. Additional studies are required to confirm whether or not this cardiovascular mobility is crucial for the pathogenesis or simply a byproduct of the cell’s ability to move within tissues and therefore inconsequential to whether or not they find the target tissues to infect. However, these results indicate that the mobility of *B. burgdorferi* contribute to its ability to find the vascular wall during extravasation.

Table of Contents

Abbreviations

BSK-II	Barbour-Stoenner-Kelly II medium
DFP	Dry-film Photoresist
GFP	Green Fluorescent Protein
PDMS	Polydimethylsiloxane
OPC	Optical Proximity Correction
SEM	Scanning Electron Microscope

1. Introduction

Borrelia burgdorferi is a vector-borne pathogen that spreads by ticks and other insects such as horse flies to a wide variety of mammalian hosts from rodents to larger animals and even humans (Burgdorfer et al., 1982; Oksi et al., 1994). As a human pathogen it is the primary cause of Lyme disease (Randolph, 2004; Johnson et al., 1984), which can develop into a chronic condition severly affecting the quality of life of the patient if not adequately treated in the initial stages of the infection (Berndtson, 2013). Symptoms can advance from fever and rash to chronic inflammation of joints and several organs (Klempner et al., 2001; Duray, 1987). Today the ticks are already the most common vector borne disease carriers in the northern hemisphere, and are projected to expand even further due to climate change (Ogden et al., 2006; Brownstein et al., 2005; Randolph, 2004). With the main carrier vector of *B. burgdorferi* growing in prevalence all around the globe the risk of Lyme disease reaching an epidemic stage in any given region is likewise on the rise. The rise of ticks as global health threats in recent years has highlighted the weaknesses in our current strategies to combat *B. burgdorferi* infections from the current diagnostics practices to the treatment protocols. The threat is further amplified by the multiple ways in which *B. burgdorferi* are able to evade immune system, which significantly hinder the control of the disease (Alitalo et al., 2001).

The immune-evasion strategies of *B. burgdorferi* begin with the mechano physical properties of the bacterial cell. *B. burgdorferi* can assume multiple pleomorphic forms depending on environmental conditions, but are most commonly found in their native spirochete configuration (Meriläinen et al., 2016). In this form *B. burgdorferi* are roughly 25 µm long 0.3 µm thin flat-wave spirochetes. The cells have have inner and outer membranes confining their cell organelles and and cytoplasm in two distinct environments. The protoplasm with all the vital cell organelles is at the center, contained within the inner membrane. Between the inner and outer membranes lies the periplasm which contains multiple flagella attached to the cell at both ends. Contracting and relaxing the flagella results in a twitching motion, which confers the bacteria an ability to swim in fluids and

tissue at the speed of up to several micrometers per second (Harman et al., 2012). This mobility is crucial for the pathogenic life cycle of *B. burgdorferi* (Sultan et al., 2013) and is what allows the bacteria to migrate from the vicinity of the initial tick bite into the vascular system and proliferate to other tissues (Kumar et al., 2015). Although the transition from the site of the tick-bite into the bloodstream may take up to two days *B. burgdorferi* is capable of leaving the cardiovascular system remarkably fast. This ability was demonstrated by Galbe et al. (1993) in an *in vivo* rat experiment where the bacteria injected into the bloodstream were able to clear from it within hours. The bacteria are able to adhere to the endothelial cell lining of the capillary veins and from there invade the tissue and move deeper. (Niddam et al., 2017). However, the ways in which *B. burgdorferi* navigate the cardiovascular system remain elusive. This can be partially attributed to the live *in vivo* observation of the cells in flow being challenging and expensive to carry out. Furthermore, it is challenging to recover the same bacterial cells for analysis once they have been injected into an *in vivo* system.

Preventing *B. burgdorferi* extravastation may be impossible in real patients due to the swiftness of this step in the pathogenic life cycle of the bacteria. However, studies into the cell mobility help to create a more complete understanding of the pathogenic life cycle of *B. burgdorferi* and potentially that of other pathogenic spirochetes. Deeper understanding of the physical characteristics of *B. burgdorferi* mobility could be applied to predict its behaviour beyond cardiovascular environments, such as computer simulations and lab-on-a-chip microfluidic systems.

Such microfluidics lab-on-a-chip systems aid in the study of microorganisms in fluid flow. In addition, the microfluidics technolgy offers numerous advantages for biological research such as minimal consumption of samples and reagents, easy integration of sample manipulation throughout the experiment, high throughput, and low cost of analysis (Ansari et al., 2013; Dongre et al., 2010; Zhu and Power, 2008). Microfluidics encompasses the domain of science studying the fluid dynamics in channels with at least one dimension below one millimeter (Whitesides, 2006). This reduction in scale causes the difference

between every-day fluid interactions and microfluidics. Compared to macroscale fluids distances and volume are reduced in microscale and surface areas increased. This causes the derived factors governing the fluid dynamics to change in prevalence. This is why in microfluidics inertial forces are less prominent, whereas viscous forces dominate the interactions (Squires and Quake, 2005). The shift in the dominance of these two forces leads to the characteristic laminar flow where fluids flow as if in organized layers according to smooth parallel paths. In such a system mixing of the layers is minimal and particles will maintain their course unless disturbed by internal or external forces. Lack of turbulent mixing can be observed in microfluidic flow in a distinct laminar flow pattern. Although mixing of the fluid occurs it is mainly caused by diffusion (Kamholz and Yager, 2001). Such microfluidic environment can be described by the complete Navier Stokes equations derived from the principles of conservation of mass, momentum, and energy (Nguyen et al., 2006). Navier Stokes equations explains the Reynolds Number as a relation of inertia divided by the viscosity. Typically with low Reynolds Numbers of one and below the fluid flows in a laminar pattern, whereas with high Reynolds Numbers of ten and above the flow is disturbed by turbulent forces. (Velve-Casquillas et al., 2010; Beebe et al., 2002) This makes Reynolds Number important to consider in microfluidic chip design in order to create desired flow patterns.

Soft-lithography is a common fabrication technique for microfluidic devices (Qin et al., 2010). The advances of recent decades in ”out of cleanroom soft lithography” has significantly cheapened fabrication of polymer based microfluidic chips. Characterizing and spreading the advantages of these cheaper and easier alternatives may be vital to the spread of the microfluidic techniques to research groups that may not have had the resources to invest in microfluidics. Microfluidic systems can be fabricated with various techniques and materials (Nguyen et al., 2006). The lithography based techniques share many similarities in the stages of their fabrication procedures. In soft-lithography the first step is the manufacturing of the mold. In clean rooms this is commonly done with electron beam lithography on SU-8 (Greiner, 2007). Outside of the cleanroom the pattern can be printed out to be used in photolithography for the mask fabrication, as illustrated in steps a-c of Figure 1.

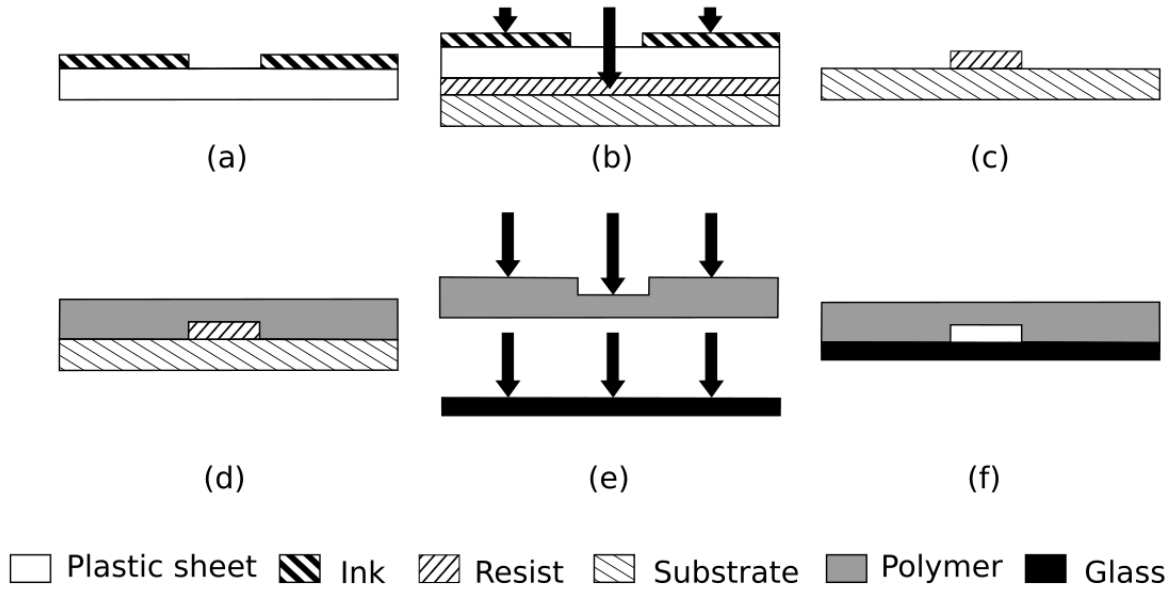

Figure 1. Schematic of microfluidic mold fabrication. Fabrication using dry film photolithography (steps a-c) and PDMS chip fabrication based soft-lithography (steps d-e). (a) A typical plastic sheet mask. (b) UV-exposure of the resist. (c) The fabricated mold after excess resist has been developed. (d) Mold is used to create an imprint in PDMS. (e) Surface of both PDMS and glass are treated with air plasma. Oxygen in the plasma creates reactive groups on the surface. (f) The treated surfaces are allowed to bond, creating a microfluidic chip.

Photolithography is a UV-light based technique where a light sensitive photoresist will absorb certain wavelengths of UV-light depending on the material of the resist. This exposed resist can then be developed in a developer to either wash away the undeveloped parts of the negative photoresist. Dry-film photoresists have recently emerged and further streamlined this step of microfluidic and microchip fabrication. Dry-film photoresists are evenly thick films from several micrometers to a hundred in thickness, which can be easily attached to a substrate such as a copper or silicon surface. However, as the resist absorbs light it also impedes with the penetration of light. This can place limitations on the absolute thickness of the photoresist and the produced structures. With dry-film photoresists the scientists can use a simple plastic sheet masks produced with regular printers as opposed to expensive chrome-film photomasks required by traditional photolithography (Stephan et al., 2007).

Once a mold has been made it can usually be used to cast several copies of the same pattern with soft lithography as depicted in step (d) of Figure 1. PDMS is the most popular material in microfluidic experiments and chip prototyping. It is a mineral-organic polymer containing both carbon and silicon in its structure. Before crosslinking the PDMS is a

highly viscous transparent fluid. A curing agent is most commonly used to crosslink it in addition to a heat treatment. PDMS retains its transparency after crosslinking which turns it into a hydrophobic elastomer. The surface of PDMS can be modified with plasma oxidation to create silanol groups on its surface, which can in turn bond with another similarly treated PDMS or glass surface, forming covalent Si-O-Si (Vlachopoulou et al., 2009) bonds as demonstrated in Figure 1 (e) and Figure 1 (f). In addition PDMS is gas permeable, which allows for in-chip cell culturing in controlled environments and has a very low autofluorescence. There are some drawbacks to PDMS however. The polymer is gas permeabley, which allows the evaporation of the liquid within the microfluidic channel (Velve-Casquillas et al., 2010). Additionally, the hydrophobicity of PDMS may cause some biomolecules to adhere to its surface. Careful consideration is therefore to be taken when balancing the possible cons of PDMS against its advantages and determining whether they are negligible compared to the advantages it offers for a microfluidic experiment or application (Mata et al., 2005).

Consequently, PDMS makes the final step of microfluidic fabrication simple. A PDMS microfluidic chip bonded with glass or another PDMS piece still needs to be connected to a macrofluidic pump or another flow setup. Because of the elasticity of the material holes can be punched into PDMS and connectors pushed in without the material breaking in the process. Glue is usually added to ensure there is no leakage. Although photolithography and plasma bonding are traditionally carried out in clean room conditions the whole process of chip manufacturing can also be done outside this room. In addition plasma bonding outside the cleanroom may trap foreign particles inside the channel, which, during the experiment, can dissolve into the sample fluid and interfere with certain types of experiments.

These microfluidic chips can be used to simulate the conditions of a cardiovascular environment without the use of animal or human test subjects. Microfluidics has certain advantages which make it particularly suitable for mimicking such complex *in vivo* environment. Active pumps connected to multiple inlets can be used to control the flow

rate of the fluid flow with unparalleled precision. The channels can be designed in such a way as to mimic the shape of the cardiovascular system. Furthermore, the lowered volume drastically reduces wastage of reagents (Wang et al., 2016). Although a microfluidic experiment setup may never be an exact copy of an *in vivo* system, it can come close to matching many physical properties of interest such as flow rate, temperature, viscocity, and structure. The physical properties defining the cardiovascular environment - viscosity, blood vessel diameter, and flow rate - can in a microfluidic experiment be controlled to imitate these properties found *in vivo*. However, unlike an *in vivo* sample, the microfluidic system is very robust, and can withstand higher concentrations of many molecules, pathogens, or nanoparticles. Microfluidic technologies thus enable the study of much larger quantities of cells at once in high throughput experiments. This allows for a more statistically reliable platform to observe general trends than its *in vivo* counterpart where similar cell concentration would prove fatal to the test subject (Velve-Casquillas et al., 2010).

2. Aims of the Study

The study had twofold objectives:

1. Characterize and optimize the parameters of a dry-film photolithography method to adapt it for use in microfluidic experiments, and to use it to fabricate microfluidic devices for bacterial flow experiments.

2. Characterize *Borrelia burdgoferi* in a microfluidic channel and potentially determine whether the physical properties of *B. burdgoferi* could be exploited by microfluidic sorting techniques.

3. Materials and Methods

3.1 Mask printing

The photolithography masks were designed with Inkscape 0.91, and exported into .png format with 2400 dpi image resolution. The images were printed on 0.1 mm thick Q-CONNECT universal inkjet transparent film with Canon Pixma iP7250 inkjet printer. In the printer settings the printing quality was set to high, the media type to photo paper pro luster, contrast to maximum, and the intensity of black to maximum.

3.2 Mold fabrication

To fabricate the mold the printed mask was pressed against a piece of DuPont Riston 200 series 38 µm thick negative photoresist laminated on copper plates by Prinel Piirilevy Oy with bullclips. The photoresist was exposed with UV-light in Stratlinker 1800 for 25 minutes on a 5 cm tall stand. The exposed photoresist was then developed with 1m/w% Na_2CO_3 at 150 rpm shaker for 8 min, and rinsed with water.

3.3 Manufacturing the microfluidic chips

To cast the chip Dow Corning Sylgard 184 Silicone Elastomer (PDMS) base and curing agent were mixed in 10:1 ratio. PDMS was poured on top of the mold to cover it with a thin (< 1 mm) layer. Bubbles were removed by placing the polymer in a vacuum chamber for 20 min. PDMS was cured at roughly 70-85°C for 1 h.

After curing, holes were punctured for inlets and outlets. PDMS and glass slide surfaces were treated using SC7620 Sputter Coater (Quorum Technologies) with purple air plasma at roughly 30-35 mA. PDMS was laid carefully against the glass slide and cured at roughly 70-85°C for 1 h.

The bases for macrofluidic connectors were prepared from small (<1 cm per side) PDMS squares cut from a 4 mm thick slab by puncturing a hole in the center. The macrofluidic

connector tubes were made by bending blunted 18-gauge syringe needles into L-shape. One tip of the L-shape was was coated with glue and pushed then into the prepared PDMS square. The glue was allowed to dry for at least 2 h.

Macrofluidic connectors were attached using the same plasma technique by treating both their underside and the top surface of the chip with plasma and placing the connectors against the inlets and outlets.

3.4 Characterization of dry photolithography

The produced masks were imaged with Leica DM5500 R/BE microscope to observe the quality of the printing. Printer settings were adjusted from the default to black-and-white with maximum contrast and black ink intensity.

For the mold fabrication both exposure time and development time were tested. Exposure time was tested by exposing grid patterns with mask containing lines of various widths from 75 µm to 500 µm. At first exposure was tested with one hour intervals between samples, then ten, until the optimal range could be found. In addition, development step was optimized by testing Na_2CO_3 concentrations between 0.8m/w% and 1.2m/w%. Shaker frequencies above 150 rpm were also tested to find the optimal conditions.

For final chip manufacturing step variations of macrofluidic connectors were tested. In one set-up the metallic tube was pressed into the chip with glue around the base. In another a small ring was added on top, which was used to cast a PDMS support around the base of the connector. Instead of using glass lide as the base for the chip a PDMS base was also tested. Different thicknesses for the top PDMS chip were also tested to find a reliably reproducible method to create less than one millimeter thin microfluidic chips with PDMS.

3.5 Culturing *Borrelia burgdorferi*

GCB726 strain of *B. burgdorferi* expressing GFP was provided by Dr. George Chaconas, University of Calgary, Canada. Cells were cultured in BSK-II (Barbour and Hayes, 1986) at 37°C in a 5% CO2 incubation closet. Experiments were carried out with cells at

relatively high concentration of 50 x 10^6 cells/ml in log phase of growth.

3.6 Laminar Flow experiment

Flow experiments were carried out using a syringe pump (New Era Syringe Pump Systems inc.) with Plastipak 1 ml syringe (Beckman Dickson). The syringes were connected to the macrofluidic connectors with syringe tubing (Beckman Dickson). All chips were initially tested for leaks with water using flow rates of up to 0.1 ml/min. The laminar flow experiment was carried out using yellow and blue food dyes and two pumps to separately control the flow rate of each inlet. The biological experiments with *B. burgdorferi* were performed with the chip placed beneath DM5500 Leica fluorescent microscope equipped with 40x objective. For visualization LED light at 470 nm wavelength was used to excite GFP within the *B. burgdorferi*. The fluorescent light intensity and gain were set to maximum in order to lower the exposure time and capture video at 4 fps. Images and video feed was captured at 0.8, 1, 2.5, 5, 10, and 20 µl/min flow rates.

4. Results

4.1 Photolithography Characterization

The initial tests with printer settings showed that the best results were obtained with the image being printed with 2400 dpi and highest possible darkness value in the printer settings. Lower darkness value used less ink and therefore let some of the UV-light through, ruining the mold with over-exposure. Q-CONNECT universal inkjet transparent film was picked as the functioning alternative for the Canon Pixma iP7250 inkjet printer. On one side it had a rough surface which helped dry the ink without the pattern being smeared. The final masks printed with the optimized settings did not exactly correspond to the schematic fed to the printer. The printed lines were not smooth due to ink droplets being several micrometers in size and often distributed in slightly skewed patterns.

In the exposure optimization the samples with below ten minute exposure time dissolved in the developer, whereas samples above twenty minutes developed normally. Samples with very high exposure time such as 2 hours had structures much wider than in the intended pattern. A steady increase in linewidth on the mold was observed with increased exposure time, correlating with the trend presented in Figure 2. A second exposure test was set up using a grid pattern with intersecting lines of increasing width from 75 µm to 300 µm. The actual line widths were then plotted against the pattern line width as illustrated in Figure 2.

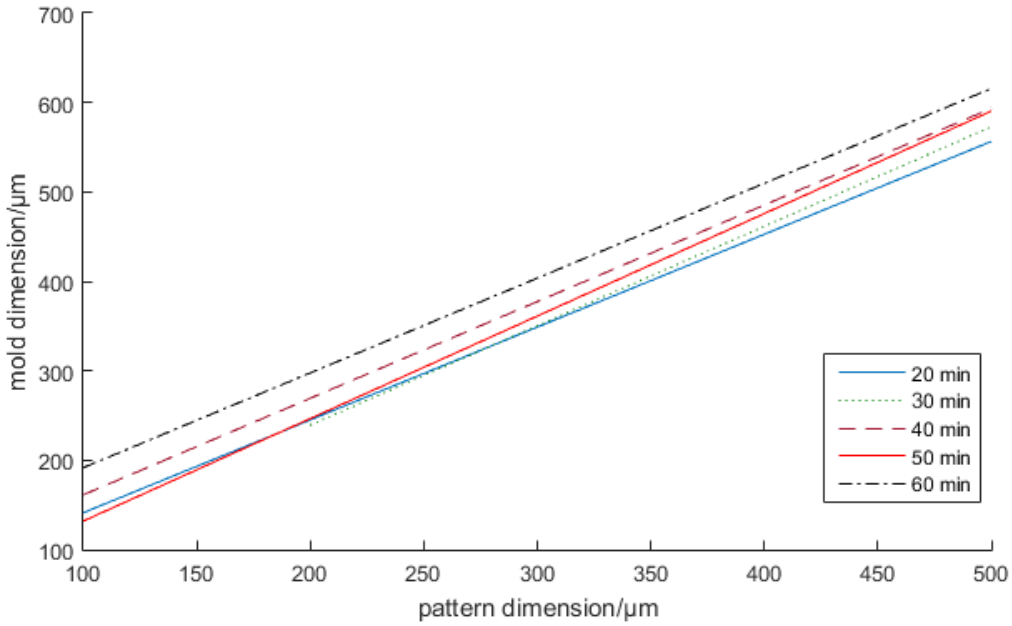

Figure 2. Relationship between pattern and mold dimension with different exposure times. Samples had lines with widths 100 µm, 200 µm, 300 µm, 400 µm, and 500 µm. Exposure time was tested with samples at 20 minutes, 30 minutes, 40 minutes, 50 minutes and 60 minutes long exposure times to gauge the range for further exposure time tests. The linewidth observed in the samples was plotted against the linewidth of the designed pattern for the different exposure times.

The 100 µm data points were omitted for 20 min samples due to their inconsistent quality, and also left out of Figure 2. Figure 2 illustrates the general trend observed in the experiments where longer exposure times would correlate with increased linewidth in the fabricated pattenr. Based on the linewidth analysis of Figure 2. additional exposure tests were carried out with the same mattern between the 20 min and 30 min range. 25 min exposure was found as the lowest exposure time at which the lowest linewidth could still be fabricated properly. In addition the linewidth with 25 minute exposure time had an acceptable correspondence between the linewidth of the pattern and the final mold as illustrated in Figure 3. and Equation 1.

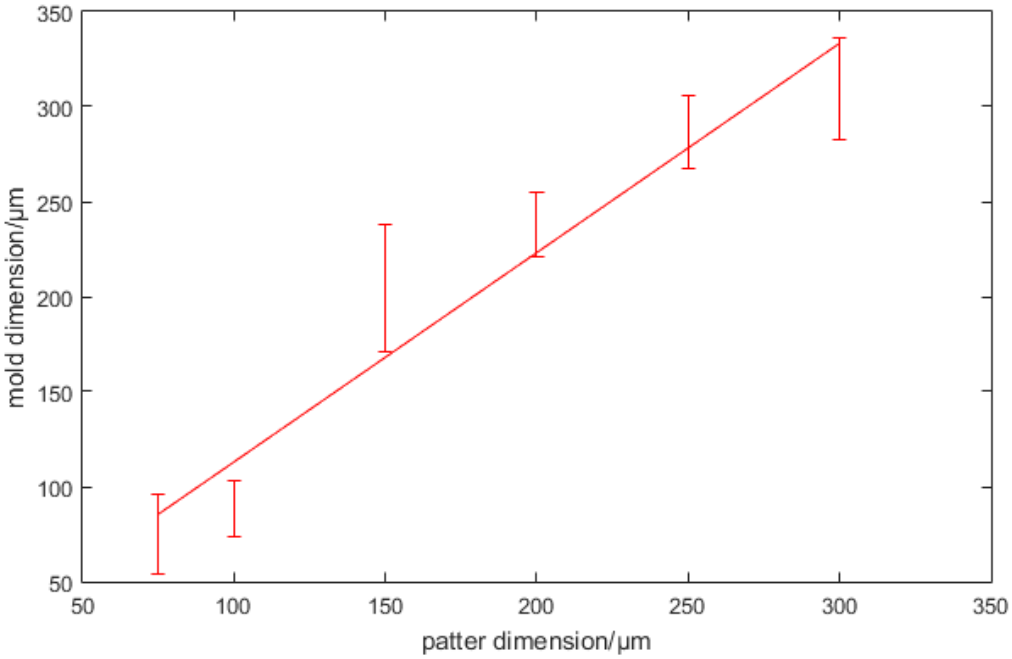

Figure 3. Relationship between pattern and mold dimension with 25 min exposure time. The average of ten measurement points for 75 µm, 100 µm, 150 µm, 200 µm, 250 µm, and 300 µm linewidths with 25 min exposure was time plotted against the actual linewidth observed in the final mold. The plotted figure had an R-square of 0.95.

75 µm the lowest resolution structure reliably replicated with the method. The mold width could be predicted using Equation 2 obtained as the linear fit of Figure 3.

$$\text{Mold width} = 1.2(\text{mask width}) + 2.8 \qquad (2)$$

The best development time was found to be the 8 minutes at 1 m/w% Na_2CO_3 as recommended in the DuPont dry-film photoresist instructions. With this time the lines developed smooth and clean without any photoresist debris sticking to them as can be observed in Figure 4. Over developing the samples resulted in even the exposed photoresist eventually detaching from the copper plate at around 25 minute mark. SEM images of fabricated molds (figures 4-5) illustrated that the ridge walls were smooth.

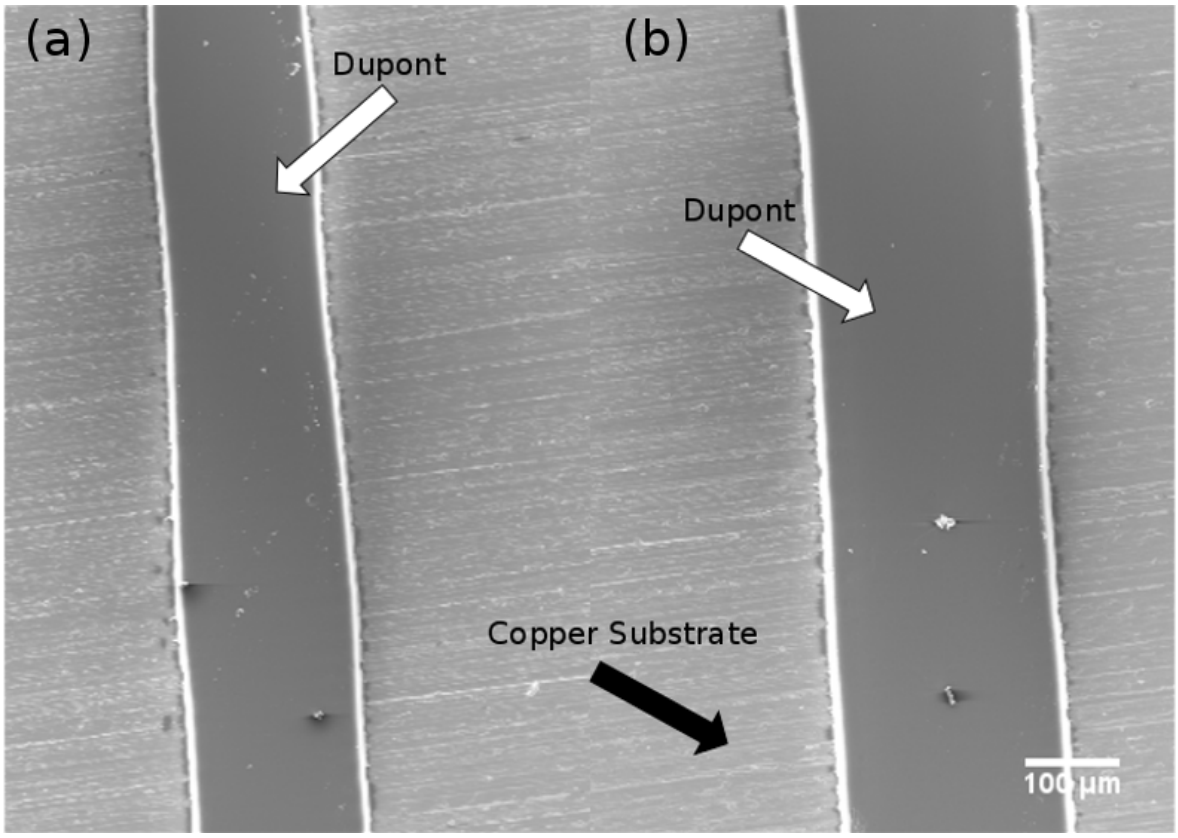

Figure 4. SEM images DuPont molds. (a) 174 µm average width ridge of DuPont dry-film photoresist. (b) 225 µm average wifth ridge of DuPont dry-film photoresist. The images were taken at 50x magnification and 10 kV electron beam voltage.

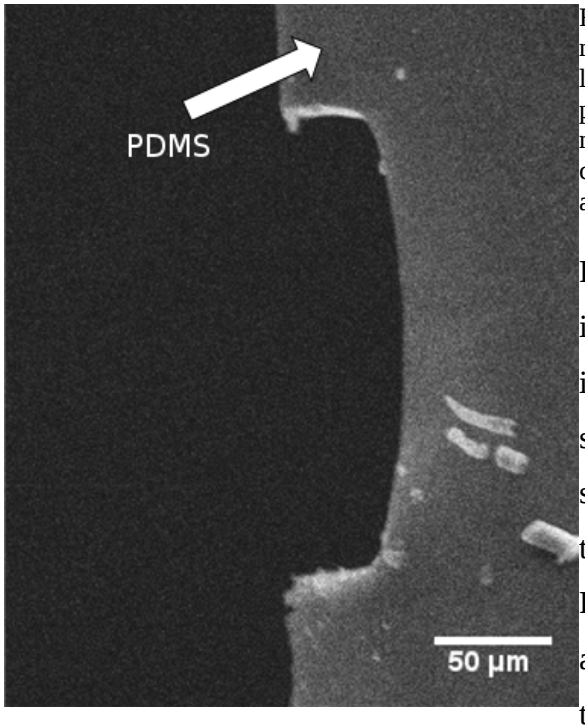

Figure 5. SEM image of a cross section of PDMS microchannel. The channel was fabricated by soft lithography after replicating from a DuPont dry-film photoresist mold. The image was obtained at 130x magnification with 30 kV electron beam voltage. The channel was ~163 µm wide with smooth channel walls and 38 µm depth at the center.

Figure 5. shows one of the cross section SEM images. In vast majority of the samples imaged with SEM the channels were very smooth and walls nearly vertical, though small bumps and fuzziness was observed on the channel walls as can be observed in Figure 4 (a) and Figure 4 (b). Furthermore, all of the samples fabricated with the technique had smoothing around the sharp

edges and near channel crossroads despite the masks having sharp angles. The curve of the channel ceiling observed in the figure 5 was also a common observation. However, some of the channels had slight curvature to them as can be observed in Figure 4 (b).

To test whether or not the minute frictions on the channel wall would interfere with the lateral flow a test was carried out with the results observed in figure 6. In the experiment set-up of Figure 6. a simple Y-channel was created with two inputs and one output. Yellow and blue food dyes were flown from the different inputs at equal flowrates to observe the laminar flow.

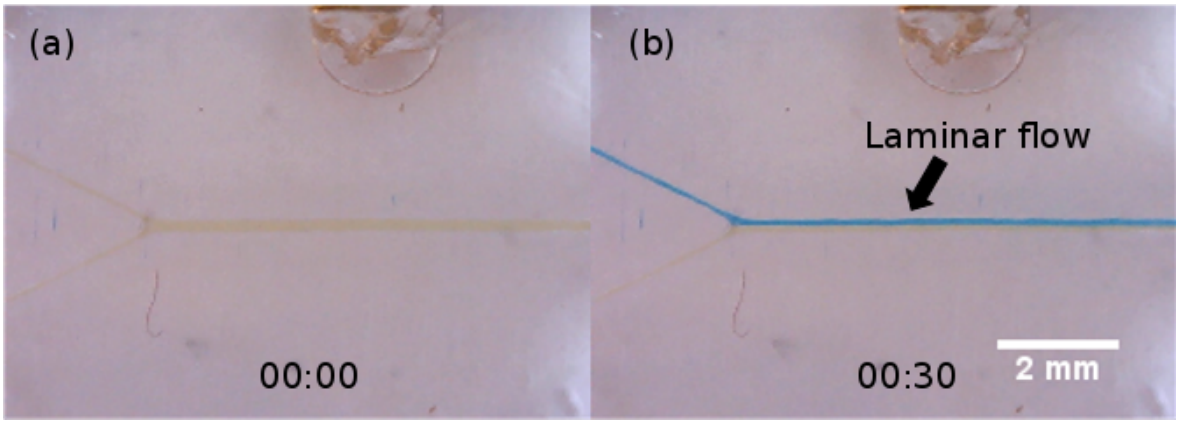

Figure 6. Laminar flow in microfluidic Y-channel. Stereo microscope images of two frames from a video captured of a flow in Y-junction microfluidic PDMS device. (a) time point 0 s depicts the device filled with yellow food dye right after the pump with blue dye is activated. (b) time point 30 s demonstrates equilibrated laminar flow after blue food dye has entered the channel.

The laminar flow of Figure 6. demonstrated in that the small fuzzy stuff at the edges of the channels depicted in Figure 4 (a) and Figure 4 (b) did not cause enough disturbance to interfere with the laminar flow. In addition, tests performed during laminar flow experiments showed that flow rates higher than 0.1 ml/min risked breaking the macrofluidic connectors or PDMS-glass bonding by starting to leak. However, there was variation in the threshold which the chips could sustain depending on how well the manual steps of the plasma bonding were carried out.

4.2 Bacteria in Microfluidic Flow

The microfluidic experiments were carried out using a single channel pattern with half-spheres on the channel walls as demonstrated by a zoomed in picture of the pattern in figure 7. The black areas depict channel wall, whereas the center white area shows where empty chanel was. The half-sphere structures were present in roughly 2 mm area in the center of the pattern. The microfluidic chip itself was a simple channel with one inlet and one outlet.

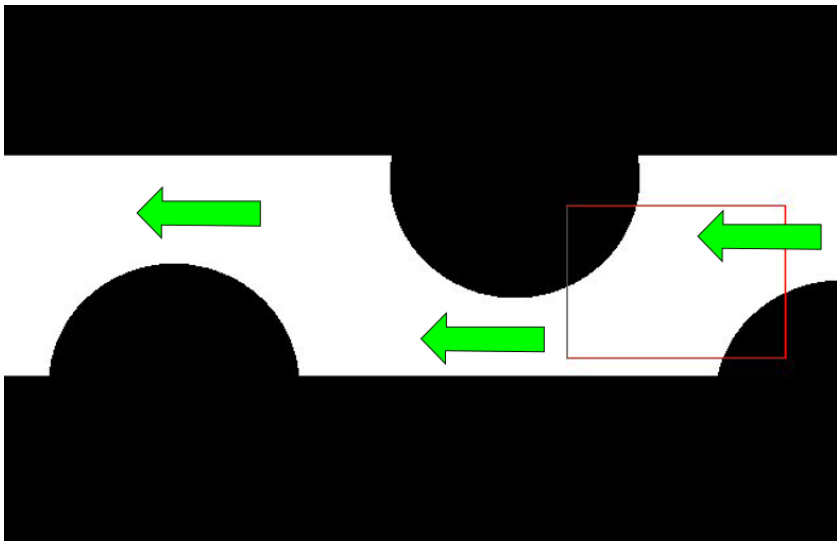

Figure 7. Zoomed in picture of the microfluidic chip pattern used in the Bacterial Flow experiments. The pattern was designed using inkscape for the experiment of Figures 8 and 9. The red square highlights the area where the images of Figures 8 and 9 are from. The channel width of the pattern was 400 µm with the spheres being 350 µm in diameter. The green arrow points towards the direction of the flow.

A stable flow was established and image recorded at 4 frames per second with various flow rates between 0 to 600 µl/h. Most of the footage from higher flow rates above 1 µl/hour was not used in the analysis as the bacteria became elongated stripes due to the low framerate. The results from 1 µl/h flow rate observed in Figures 8 and 9. Figure 8. depicts *B. burgdorferi* in the channel structure depicted in Figure 7. To compare the fluid speed with that of human capillaries it was calculated. The fluid speed at the center of the channel was calculated from the footage of Figure 8. by tracking cells to be roughly 0.0073 cm/s as

demonstrated with the cell highlighted with red circle in Figure 8.

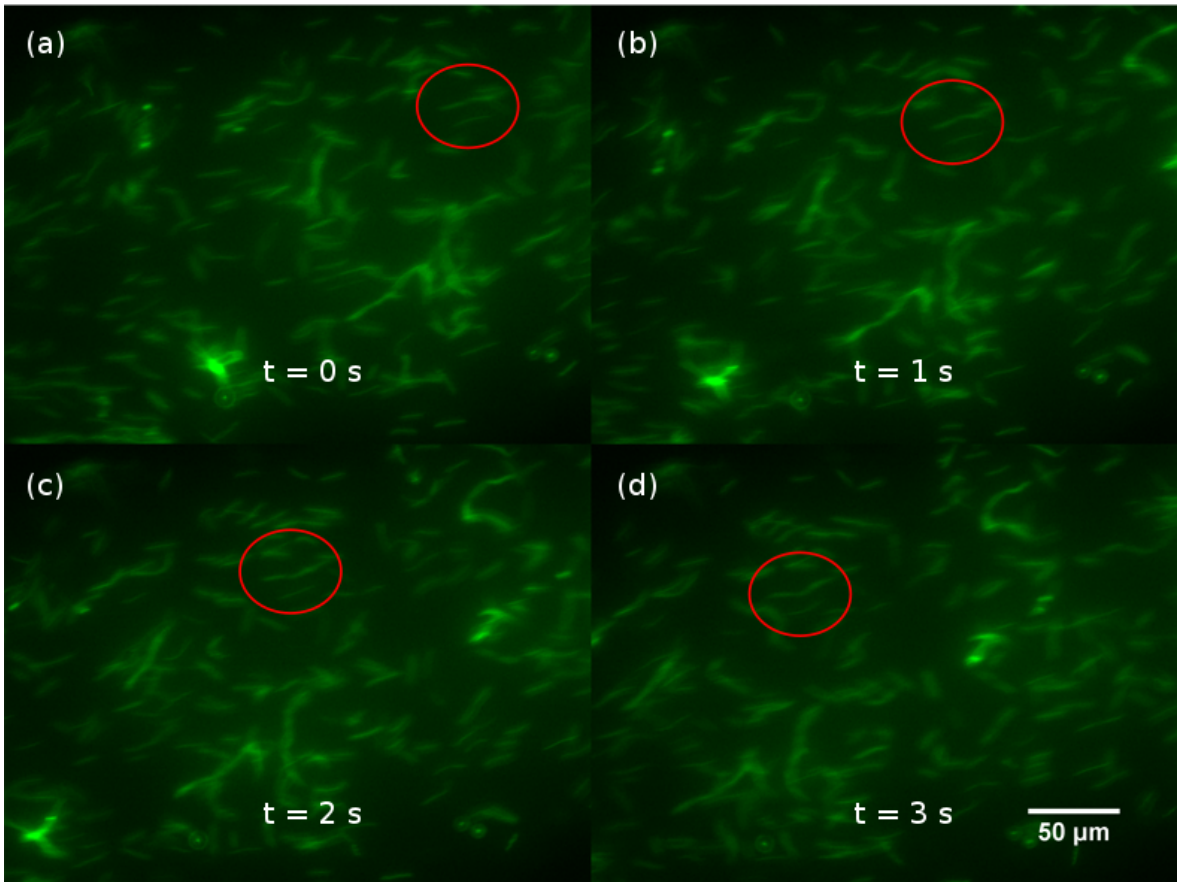

Figure 8. Still frames from footage of flwoing *B. burgdorferi* in a microfluidic chip. *B. Burgdorferi* flow at 1 µl/h from right to left. Images were obtained with 40 x magnification. (a) A still frame from timepoint 0 s. The highlighted cell can be seen at the top the observation area. (b) A still frame of time point 1 s. The highlighted cell has moved. (c) A still frame of timepoint 2 s. The highlighted cell has moved and changed its orientation. (d) A still frame of timepoint 3 s. The highlighted cell has continued moving with the flow and tilted further.

Figure 8. (a-d) demonsrtate that the shape and movement of individual *B. burgdorferi* can be observed clearly at 1 µl/h flowrate. The borrelia did not flow in a uniform pattern, but instead at various angles as can be observed in Figure 8. (d) where the cell in front of the highlighted cell is flowing perpendicular to the direction of the flow. Many of the bacteria also exhibited some types of movement aside from the flow such as ’dancind’ and flipping motions. The types of motile behaviour observed in the footage could be separated into three main categories detailed in Figure 9.

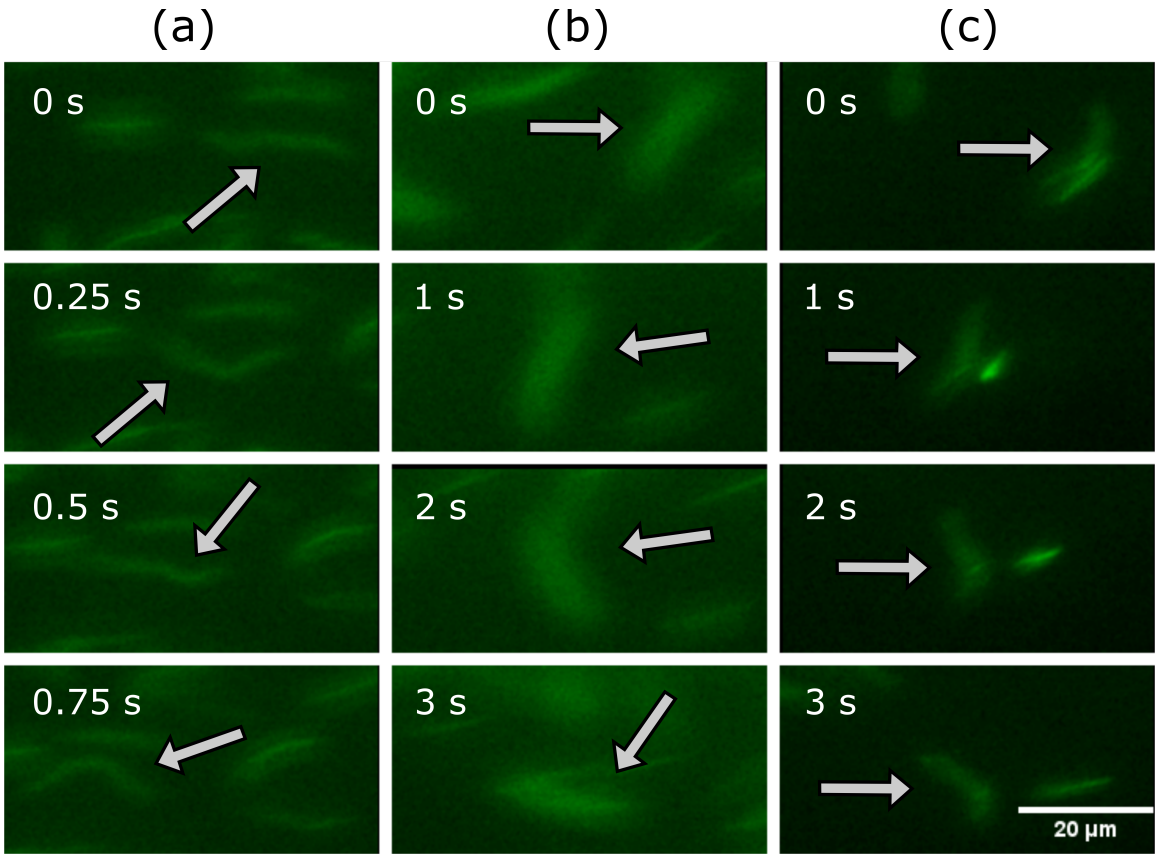

Figure 9. Image montages of the observed motility types in three image montage columns. The image series are read from top to bottom. (a) *B. burgdorferi* dancing. Same cell tracked over four seconds is depicted exhibiting ’dancing’ motions in the flow. (b) *B. burgdorferi* flipping. The highlighted cell flips over 90 degrees in the flow by itself. (c) *B. burgdorferi* interacting with the wall. The highlighted cell flips as it comes to contact with the wall of the microfluidic channel.

The mobility types listed in Figure 9 were exhibited by nearly all of the observed bacteria to varying extents. The frequency of the motility modes depicted in Figure 9. were not observed continuously in all *B. Burgdorferi* as some could stay still for nearly the full length of the field of view without moving, and then spring into rapid ’dancing’ motions.

5. Discussion

Both the dry-film photolithography technique and biological experiment gave answers to the proposed research questions. Optimizing the exposure and development parameters was necessary for achieving as high resolution as possible for photolithography as many microfluidic techniques require a sufficiently small resolution structures to work. Many of the obstacles initially faced in the photolithography optimization such as poor mask quality, were overcome. The remaining ones – fuzziness of the channel wall, and slight bending of channels - were either intrinsic to the dry-film-photolithography technique used or would require higher quality equipment and reagents such as photoplotter, and thinner dry-film photoresist. However, the dry-film photolithography method could in the end be used to produce different kinds of microfluidic chips for both microscopical biological and for regular flow experiments as seen in Figures 5, 6, and 7. B.

The channel bending observed during the exposure optimization and in Figure 4. occurred due to the method with which the mask and photoresist were secured being closer to proximity printing than contact printing. In proximity lithography method there is a distance between the mask and the photoresist, whereas in contact printing the mask is set up in tight physical contact against the photoresist (THOMPSON, 1983). A known issue with proximity lithography printing is the diffraction occurring between the mask and the photoresist, which lowers the resolution of the fabricated structure. Furthermore, inkjet printing techniques have a resolution limit of 70 to 120 μm (Nguyen et al., 2006). Despite this, an unexpected observation made at the beginning of the study was how relatively bad quality masks could still be used in the exposure step to fabricate molds with much higher quality channel walls than what were observed on the printed mask. The ink droplets of the mask were visible under the microscope, but smoothed out in the molds and PDMS chips manufactured with the masks. This was attributed partially to light scattering in the plastic sheet after passing the ink, in the protective plastic sheet on top of dupont, and once more within the photoresist itself. Furthermore, the ink itself could not perfectly block all light as as samples given UV-exposure of 60 minute and above had all of the photoresist fully

exposed. A portion of the light was blocked by the ink, but some got through. In combination with the light scattering this was likely enough to finish exposing photoresist around the edges of the pattern. However, because the light was able to partially penetrate the mask a rounding effect was observed in sharp corners and crossroads of the channels. This ultimately prevented the accurate fabrication of sharp angles and shapes such as squares, though OPC techniques may offer way to partially overcome this limitation (Du et al., 1999). OPC method aims to compensate for the rounding of the edges by stretching out the corners to be pointier and narrower. OPC can be adapted as either model, or rule based technique. Model based OPC can be time consuming as the corrections to patterns are adapted by trial and error, whereas rule based is, as the name implies, based on sets of mathematical rules (Puthankovilakam, 2017).

The slight curving of the channel observed in Figure 4. was caused by more mundane culprit. The mask not being perfectly aligned against the substrate during the exposure due to them being attached manually using bull-clips. Much of this could be compensated for by taking caution when attaching the mask against the substrate, but microscale mis-alignments were difficult to account for. The line edge roughness observed in the masks at the edges of the channels could not be wholly removed during the optimization procedures. These types of defects should be attributed to particles trapped between the mask and the photoresist, which is plausible considering that the microfluidic fabrication steps presented in this thesis were carried out outside of the cleanroom. However, as mentioned before these issues were deemed minor as the defects were not sufficient to disturb the laminar flow, as seen in Figure 6.

Dry-film photolithography remains in high popularity due to its relatively low cost and ease of use. Although new advanced materials allow up to nanometer scale fabrication, the resolution limit for traditional films sits at around few micrometers with especially thin photoresists and low wavelength light sources (Furuya et al., 2015). For our fabrication method the resolution could potentially be further enhanced down to 10 µm range by creating an exposure setup with perfect contact lithography, by creating the masks with a photoplotter rather than an inkjet office printer, and by employing thinner photoresist to

reduce the effect of diffraction. However, improving the mask quality by switching from inkjet printing to photoplotters may not be feasible to achieve with equipment found in most biological laboratories as the photoplotter devices cost above 10, 000 €. Regardless, dry-film photolithography can be used to an extent even without expensive equipment as seen in the thesis. All the steps of chip manufacturing covered in the materials and methods section could be carried out with material costs of less than one euro within the span of roughly 5 hours outside of an expensive cleanroom. Moreover, multiple chips could be fabricated at once. With this a scientist could design a microfluidic experiment set-up, or multiple variations of it, and carry out the experiments on the following day.

The erratic movement of borrelia observed in the Figures 7 and 8 for the most part can be attributed to the intrinsic motility of *B. burgdorferi.* Particles in laminar flow normally carry out on a set path, but in the case of highly motile particles such as *B. burgdorferi* the bacteria may bend and twist to move itself from one laminar layer to the next. The small defects on present in the channel wall did not visibly disturb the laminar flow as confirmed by laminar flow tests seen in Figure 6, but they could potentially have been enough to cause small pockets of turbulence near the walls. Furthermore, it is possible that these turbulences could have also affected cells not in the direct contact with the wall. Due to the dominance of viscous forces in a microfluidic environment the flow near the walls is also slower closer to the wall. Fluid flow in the channel could be described with a parabolic flow profile. In the center the bacteria are able to swim freely without shear force affecting them (Nguyen et al., 2006). Strong shear force near the wall can cause long particles that extend from laminar layer to the next, such as *B. burgdorferi*, to get ’shear trapped’ (Son et al., 2015). Consequently, the observed flipping is likely caused by uneven torque applied by the the flow on the elongated *B. burgdorferi* cells. The phenomena of elongated cells experiencing so called Jeffey orbits in shear conditions is well documented (Kaya and Koser, 2009; Son et al., 2015). may have been partially caused by the fluid flow itself. However, the ’dancing’ motion presented in Figure 9 (a) may enable *B. Burgdorferi* to alter its orientation actively.

Although, the experimental conditions presented in this thesis differed from *in vivo* in

many aspects, they sought to imitate certain physical conditions of the cardiovascular system. The fluid velocity at which most of the recordings were made was roughly one third of the 0.03 cm/s flow speed of the blood in human capillary vessels. Since the flow experiments were performed in BSK-II media rather than whole blood the fluid viscosity of the experiments was also slightly lower (Marieb and Hoehn). In essence this means that the movements observed in our experiments are slightly slower compared to how the bacteria move inside an actual blood vessel due to sphirochetes generally moving faster in more viscious media (Li et al., 2010). The effect of slowed flow near the wall of the channel likewise persists in cardiovascular system. Based on the observed results a hypothesis for how the borrelia navigate the blood vessels can be drawn. Upon entering the cardiovascular system the bacteria retain their mobility, and by twitching they are able to naturally gravitate towards the wall of the blood vessel. Due to the flow being much slower at the wall and the shear trapment (Son et al., 2015) keeping the cells near it the bacteria are able to anchor themselves to the endothelial tissue by tethers using plasma fibronectin (Niddam et al., 2017). *B. burgdorferi s*urface proteins vital for this tethering step in the extravasation. Studies suggests that bacterial mobility is also essential for the pathogenic life cycle of *B. Burgdorferi* (Sultan et al., 2013). However, it has not been clear whether motility plays a role in both vascular and soft tissue navigation. Our results suggest that the motility of *B. burgdorferi* may help the bacteria move within the blood flow by ’dancing’ to actively change its orientation.

6. References

Alitalo, A., T. Meri, L. Rämö, T.S. Jokiranta, T. Heikkilä, I.J.T. Seppälä, J. Oksi, M. Viljanen, and S. Meri. 2001. Complement evasion by Borrelia burgdorferi: Serum-resistant strains promote C3b inactivation. *Infect. Immun.* 69:3685–3691. doi:10.1128/IAI.69.6.3685-3691.2001.

Ansari, K., J.Y.S. Ying, P.C. Hauser, N.F. de Rooij, and I. Rodriguez. 2013. A portable lab-on-a-chip instrument based on MCE with dual top-bottom capacitive coupled contactless conductivity detector in replaceable cell cartridge. *Electrophoresis*. 34:1390–1399. doi:10.1002/elps.201200592.

Barbour, a G., and S.F. Hayes. 1986. Biology of Borrelia species. *Microbiol. Rev.* 50:381–400.

Beebe, D.J., G.A. Mensing, and G.M. Walker. 2002. Physics and Applications of Microfluidics in Biology. *Annu. Rev. Biomed. Eng.* 4:261–286. doi:10.1146/annurev.bioeng.4.112601.125916.

Berndtson, K. 2013. Review of evidence for immune evasion and persistent infection in Lyme disease. *Int. J. Gen. Med.* 291. doi:10.2147/IJGM.S44114.

Brownstein, J.S., T.R. Holford, and D. Fish. 2005. Effect of climate change on lyme disease risk in North America. *Ecohealth*. 2:38–46. doi:10.1007/s10393-004-0139-x.

Burgdorfer, W., A.G. Barbour, S.F. Hayes, J.L. Benach, E. Grunwaldt, and J.P. Davis. 1982. Lyme disease-a tick-borne spirochetosis? *Science*. 216:1317–1319. doi:10.1126/science.7043737.

Dongre, C., J. van Weerd, G.A.J. Besselink, R. van Weeghel, R.M. Vazquez, R. Osellame, G. Cerullo, M. Cretich, M. Chiari, H.J.W.M. Hoekstra, and M. Pollnau. 2010. High-resolution electrophoretic separation and integrated-waveguide excitation of fluorescent DNA molecules in a lab on a chip. *Electrophoresis*. 31:2584–2588. doi:10.1002/elps.201000126.

Du, J., Q. Huang, J. Su, Y. Guo, and Z. Cui. 1999. New approaches to optical proximity correction in photolithography. *Microelectron. Eng.* 46:73–76. doi:10.1016/S0167-9317(99)00018-0.

Duray, P.H.M.D. 1987. The Surgical Pathology of Human Lyme Disease: An Enlarging Picture. *Am. J. Surg. Pathol.* The Arthur.

Furuya, R., H. Lu, F. Liu, H. Deng, T. Ando, V. Sundaram, and R. Tummala. 2015.

Demonstration of 2μm RDL wiring using dry film photoresists and 5μm RDL via by projection lithography for low-cost 2.5D panel-based glass and organic interposers. *Proc. - Electron. Components Technol. Conf.* 2015–July:1488–1493. doi:10.1109/ECTC.2015.7159794.

Galbe, J.L., E. Guy, J.M. Zapatero, E.I. Peerschke, and J.L. Benach. 1993. Vascular clearance of Borrelia burgdorferi in rats. *Microb Pathog*. 14:187–201. doi:S0882-4010(83)71019-3 [pii]\r10.1006/mpat.1993.1019.

Greiner, A. del C. and C. 2007. SU-8: a photoresist for high-aspect-ratio and 3D submicron lithography. *J. Micromechanics Microengineering*. 17.

Harman, M.W., S.M. Dunham-Ems, M.J. Caimano, a. a. Belperron, L.K. Bockenstedt, H.C. Fu, J.D. Radolf, and C.W. Wolgemuth. 2012. The heterogeneous motility of the Lyme disease spirochete in gelatin mimics dissemination through tissue. *Proc. Natl. Acad. Sci.* 109:3059–3064. doi:10.1073/pnas.1114362109.

Johnson, R.C., G.P. Schmid, F.W. Hyde, and A.G. Steigerwalt. 1984. Borrelia burgdorferi sp. nov.: Etiologic Agent of Lyme Disease. *Int. J. Syst. Bacteriol.* 496–497. doi:10.1099/00207713-34-4-496.

Kamholz, A.E., and P. Yager. 2001. Theoretical Analysis of Molecular Diffusion in Pressure-Driven Laminar Flow in Microfluidic Channels. *Biophys. J.* 80:155–160. doi:10.1016/S0006-3495(01)76003-1.

Kaya, T., and H. Koser. 2009. Characterization of Hydrodynamic Surface Interactions of Escherichia coli Cell Bodies in Shear Flow. *Phys. Rev. Lett.* 103:138103. doi:10.1103/PhysRevLett.103.138103.

Klempner, M.S., L.T. Hu, J. Evans, C.H. Schmid, G.M. Johnson, R.P. Trevino, D. Norton, L. Levy, D. Wall, J. McCall, M. Kosinski, and A. Weinstein. 2001. Two controlled trials of antibiotic treatment in patients with persistent symptoms and a history of Lyme disease. *N. Engl. J. Med.* 345:85–92. doi:10.1056/NEJM200107123450202.

Kumar, D., L.C. Ristow, M. Shi, P. Mukherjee, J.A. Caine, W.Y. Lee, P. Kubes, J. Coburn, and G. Chaconas. 2015. Intravital Imaging of Vascular Transmigration by the Lyme Spirochete: Requirement for the Integrin Binding Residues of the B. burgdorferi P66 Protein. *PLoS Pathog.* 11. doi:10.1371/journal.ppat.1005333.

Li, C., H. Xu, K. Zhang, and F.T. Liang. 2010. Inactivation of a putative flagellar motor switch protein FliG1 prevents Borrelia burgdorferi from swimming in highly viscous media and blocks its infectivity. *Mol. Microbiol.* 75:1563–1576. doi:10.1111/j.1365-2958.2010.07078.x.

Marieb, E.N., and K. Hoehn. Human Anatomy & Physiology Ninth Edition. 9th ed.

Pearson.

Mata, A., A.J. Fleischman, and S. Roy. 2005. Characterization of polydimethylsiloxane (PDMS) properties for biomedical micro/nanosystems. *Biomed. Microdevices*. 7:281–293. doi:10.1007/s10544-005-6070-2.

Meriläinen, L., H. Brander, A. Herranen, A. Schwarzbach, and L. Gilbert. 2016. Pleomorphic forms of Borrelia burgdorferi induce distinct immune responses. *Microbes Infect.* 18:484–495. doi:10.1016/j.micinf.2016.04.002.

Nguyen, N.-T., S.T. Wereley, and A. Rtechhouse. 2006. Fundamentals and Applications of Microfluidics. 2nd editio. Artech House. 512 pp.

Niddam, A.F., R. Ebady, A. Bansal, A. Koehler, B. Hinz, and T.J. Moriarty. 2017. Plasma fibronectin stabilizes Borrelia burgdorferi–endothelial interactions under vascular shear stress by a catch-bond mechanism. *Proc. Natl. Acad. Sci.* 201615007. doi:10.1073/PNAS.1615007114.

Ogden, N.H., A. Maarouf, I.K. Barker, M. Bigras-Poulin, L.R. Lindsay, M.G. Morshed, C.J. O'Callaghan, F. Ramay, D. Waltner-Toews, and D.F. Charron. 2006. Climate change and the potential for range expansion of the Lyme disease vector Ixodes scapularis in Canada. *Int. J. Parasitol.* 36:63–70. doi:10.1016/j.ijpara.2005.08.016.

Oksi, J., I. Helander, H. Aho, M. Marjamäki, and M.K. Viljanen. 1994. Borrelia Burgdorferi Shown By PCR from Skin Biopsy Specimen after a Fly Bite. *In* Lyme Borreliosis. 45–48.

PUTHANKOVILAKAM, K. 2017. Limitations of Proximity Lithography Printing: Simulations, Experiments, and Applications.

Qin, D., Y. Xia, and G.M. Whitesides. 2010. Soft lithography for micro- and nanoscale patterning. *Nat. Protoc.* 5:491–502. doi:10.1038/nprot.2009.234.

Randolph, S.E. 2004. Evidence that climate change has caused "emergence" of tick-borne diseases in Europe? *Int. J. Med. Microbiol.* 293:5–15. doi:http://dx.doi.org/10.1016/S1433-1128(04)80004-4.

Son, K., D.R. Brumley, and R. Stocker. 2015. Live from under the lens: exploring microbial motility with dynamic imaging and microfluidics. *Nat. Rev. Microbiol.* 13:761–775. doi:10.1038/nrmicro3567.

Squires, T.M., and S.R. Quake. 2005. Microfluidics: Fluid physics at the nanoliter scale. *Rev. Mod. Phys.* 77:977–1026. doi:10.1103/RevModPhys.77.977.

Stephan, K., P. Pittet, L. Renaud, P. Kleimann, P. Morin, N. Ouaini, and R. Ferrigno. 2007. Fast prototyping using a dry film photoresist: microfabrication of soft-lithography

masters for microfluidic structures. *J. Micromechanics Microengineering*. 17:N69–N74. doi:10.1088/0960-1317/17/10/N01.

Sultan, S.Z., A. Manne, P.E. Stewart, A. Bestor, P.A. Rosa, N.W. Charon, and M.A. Motaleba. 2013. Motility is crucial for the infectious life cycle of borrelia burgdorferi. *Infect. Immun.* 81:2012–2021. doi:10.1128/IAI.01228-12.

THOMPSON, L.F. 1983. An Introduction to Lithography. 1–13.

Velve-Casquillas, G., M. Le Berre, M. Piel, and P.T. Tran. 2010. Microfluidic tools for cell biological research. *Nano Today*. 5:28–47. doi:10.1016/j.nantod.2009.12.001.

Vlachopoulou, M.-E., A. Tserepi, P. Pavli, P. Argitis, M. Sanopoulou, and K. Misiakos. 2009. A low temperature surface modification assisted method for bonding plastic substrates. *J. Micromechanics Microengineering*. 19:15007. doi:10.1088/0960-1317/19/1/015007.

Wang, L., W. Liu, S. Li, T. Liu, X. Yan, Y. Shi, Z. Cheng, and C. Chen. 2016. Fast fabrication of microfluidic devices using a low-cost prototyping method. *Microsyst. Technol.* 22:677–686. doi:10.1007/s00542-015-2465-z.

Whitesides, G.M. 2006. The origins and the future of microfluidics. *Nature*. 442:368–373. doi:10.1038/nature05058.

Zhu, Y., and B.E. Power. 2008. Lab-on-a-chip in Vitro Compartmentalization Technologies for Protein Studies. 81–114.